



# A long simultaneous XMM-NuSTAR look of MCG-6-30-15

Andrea Marinucci (Roma Tre)

G. Matt, G. Miniutti, L. Brenneman,  
M. Guainazzi, A. Fabian, M. Parker  
and the NuSTAR AGN Physics WG

Santorini

Explosive transients: lighthouses of the Universe  
September 16<sup>th</sup>, 2013

# Overview

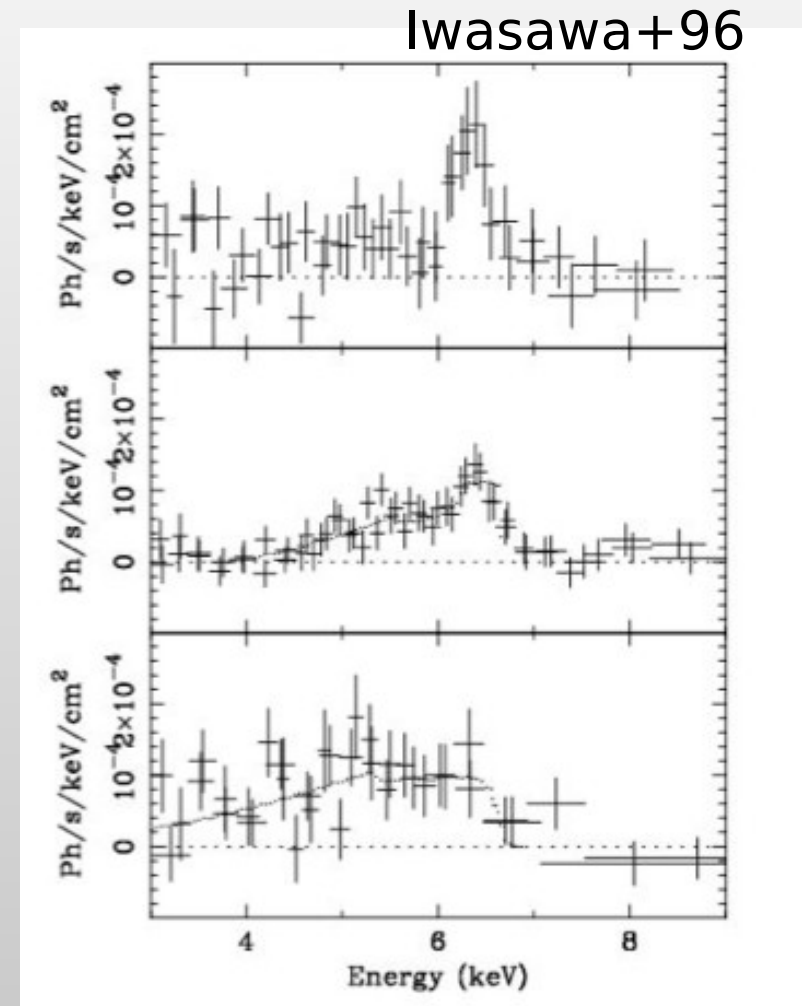
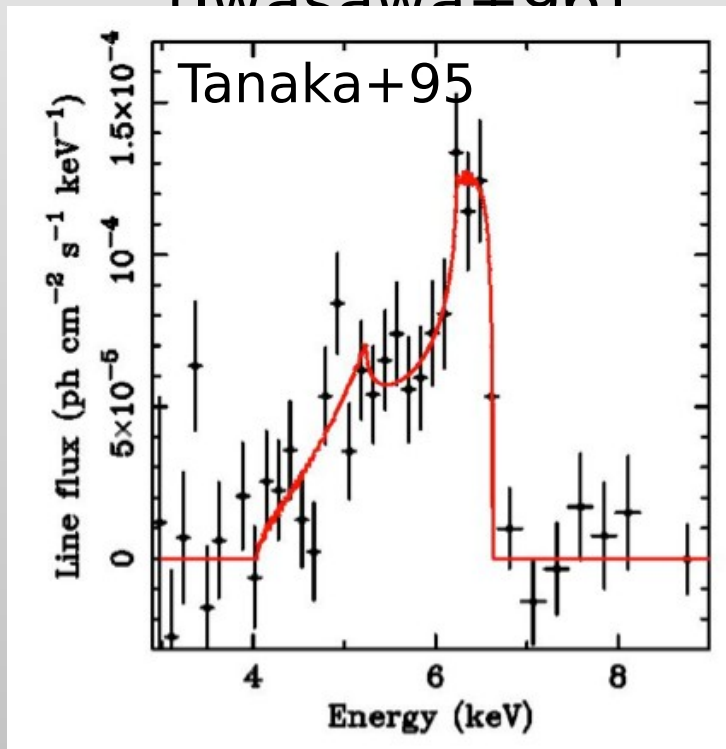
- Brief introduction on MCG-6-30-15
- The XMM-NuSTAR 2013 observational campaign
  - Testing the two different scenarios
    - Results
- Conclusions and future perspectives

# Overview

- Brief introduction on MCG-6-30-15
- The XMM-NuSTAR 2013 observational campaign
  - Testing two different scenarios
    - Results
- Conclusions and future perspectives

# Introduction

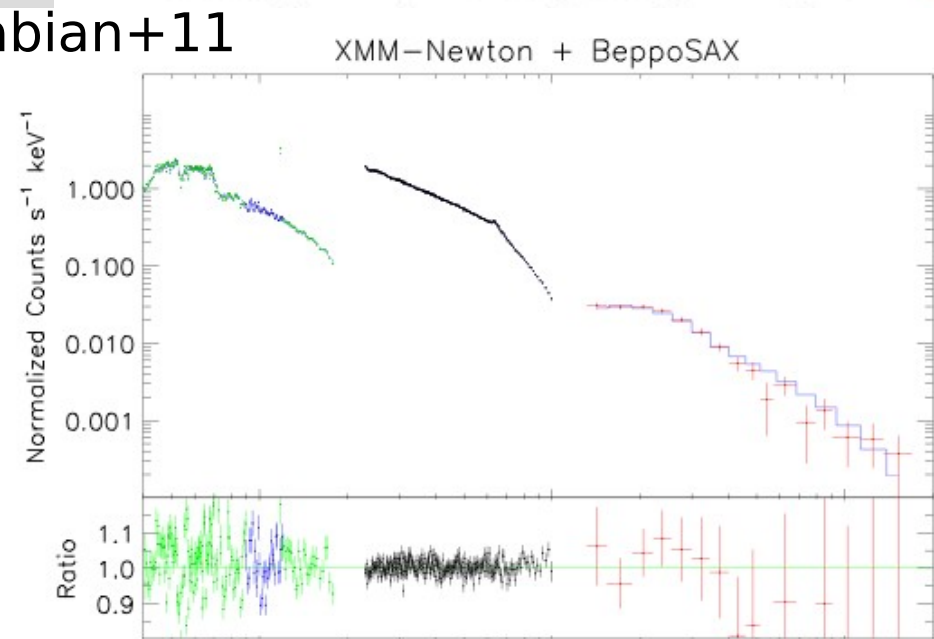
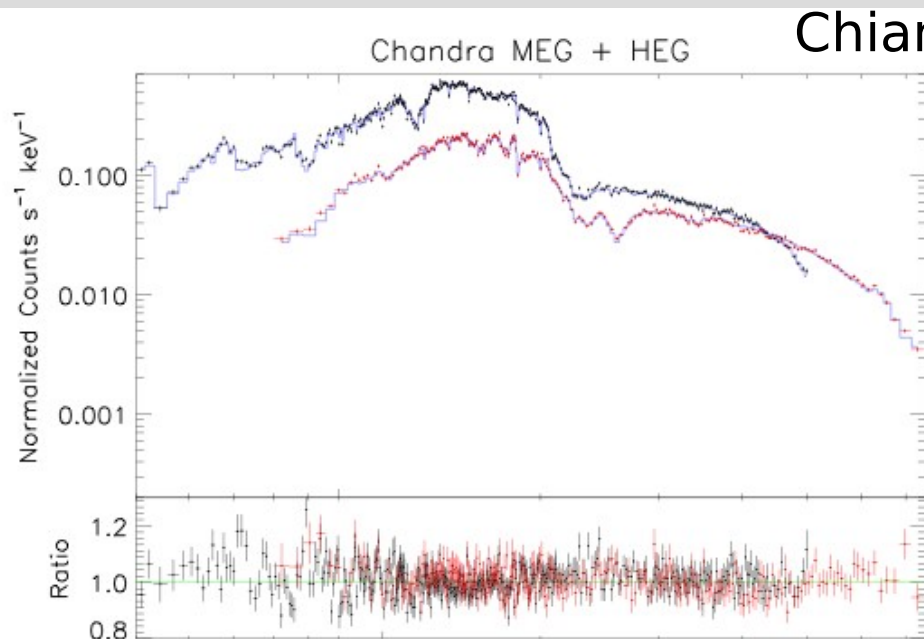
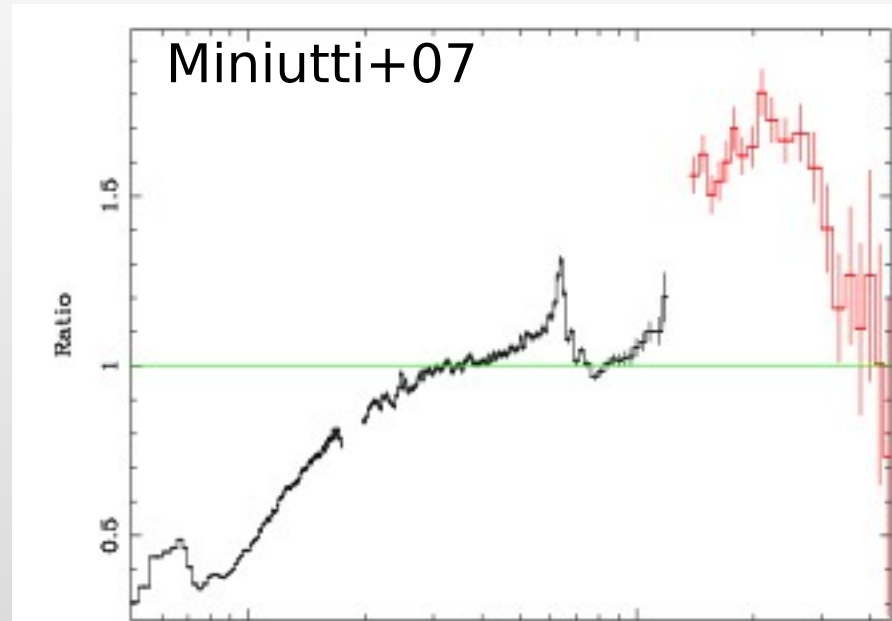
Bright Sy 1 galaxy hosting the first broad Fe  $K\alpha$  line ever observed (Tanaka+95) and interpreted as originating from a rapidly spinning BH (Iwasawa+96)



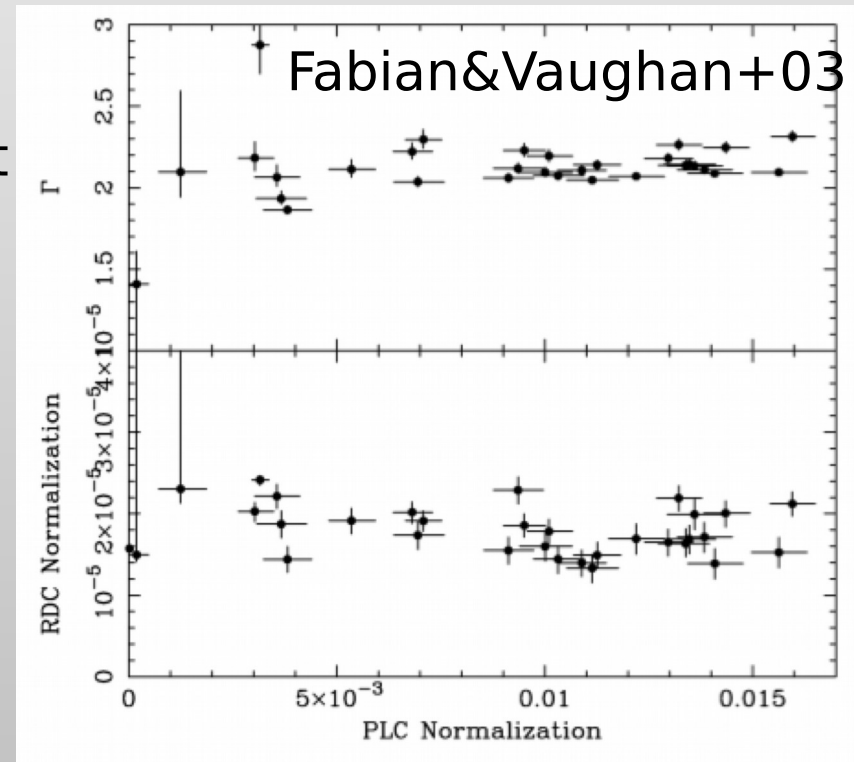
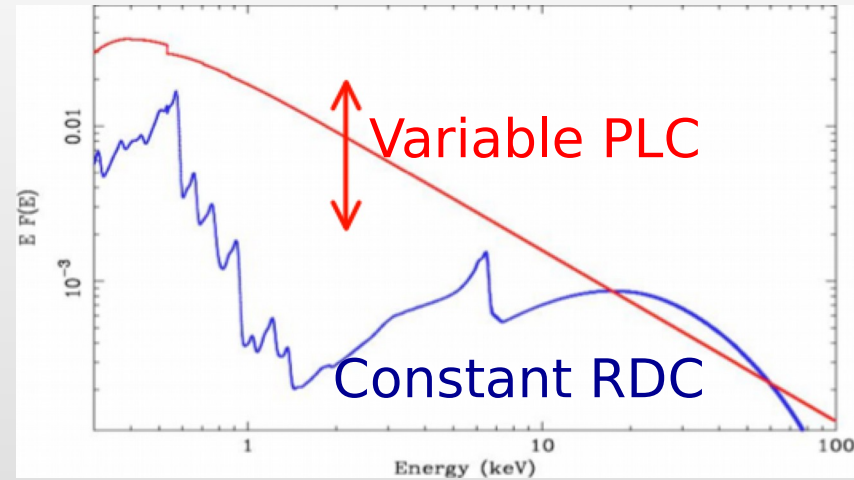
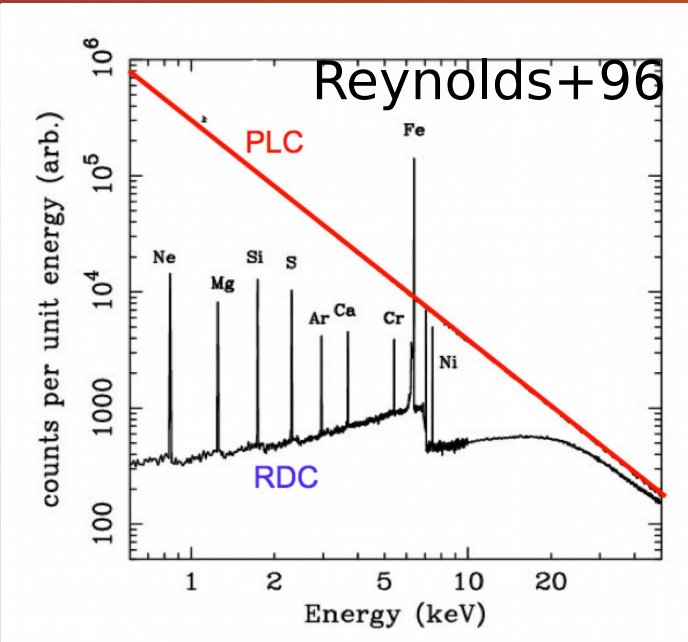
# X-ray observations

Extensively observed in the X-rays:

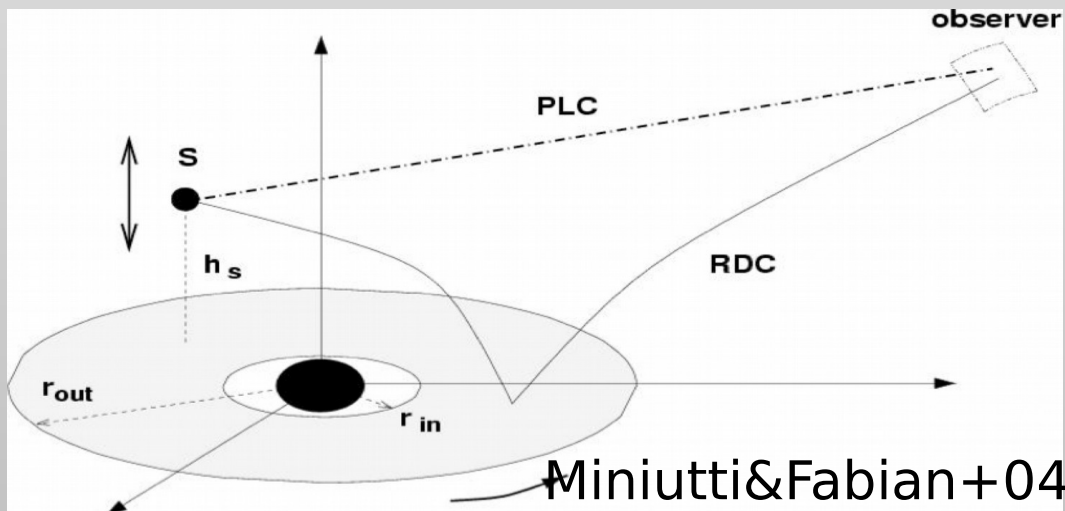
- complex absorption (Lee+01, Chiang&Fabian+11)
- strong reflection hump (Miniutti+07)
- very broad Fe Ka line (Brenneman&Reynolds+06)



# Reflection scenario

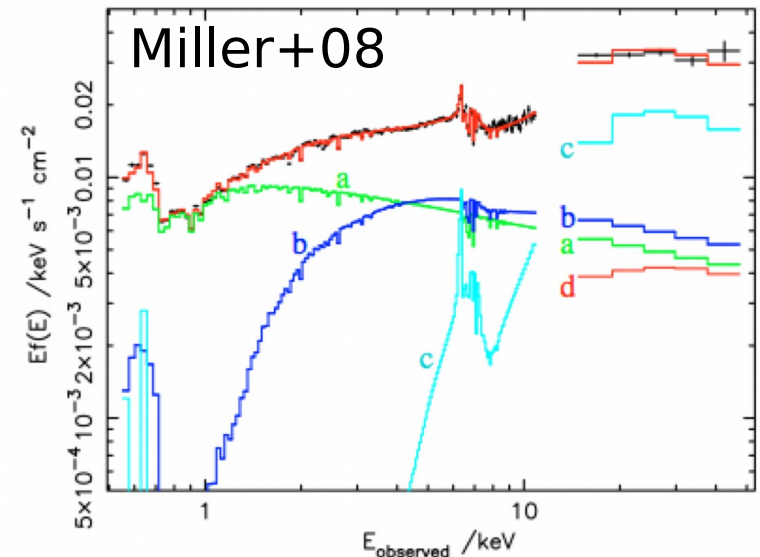
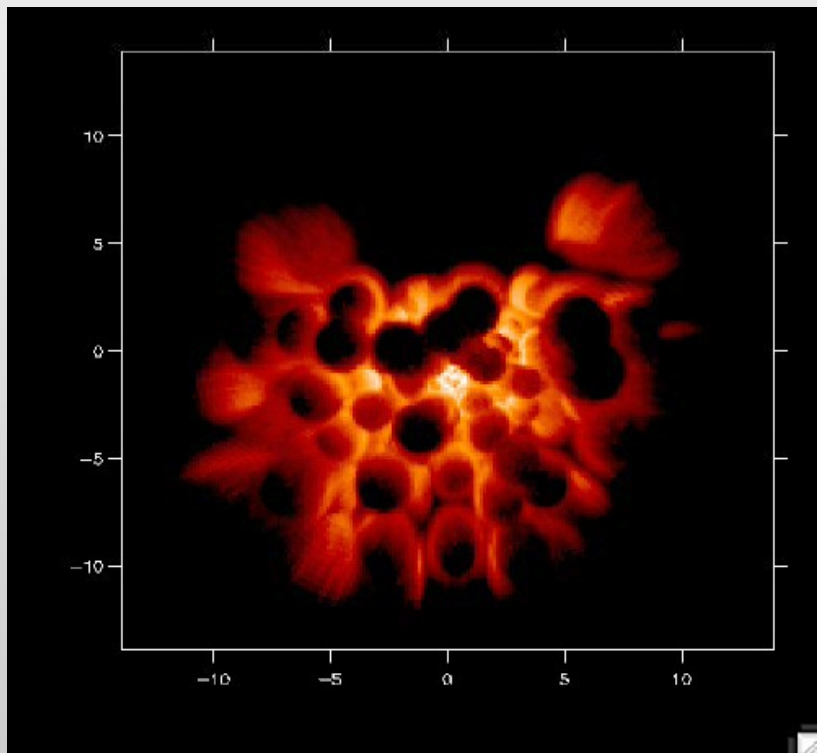


Light bending model: much of the flux is bent onto the disk giving a constant, strong RDC



# Absorption scenario

An alternative interpretation explains the spectral variability in terms of absorption changes



**“3+2” MODEL**  
 Fig. 4. Illustration of the spectral model. The upper curve shows the model fitted to the mean *Suzaku* spectrum, with XIS data below 11 keV and PIN data above 15 keV. Points with error bars show the unfolded data (see Sec. 4 for details). The three emission components are shown as (a) primary directly-viewed power-law, absorbed by zones 1 and 2; (b) partially covered power-law, absorbed by zones 1, 2, 3 and 5; (c) reflection, absorbed by zones 1, 2, 3 and 4. In the fit to the PCA components, zone 3 is excluded from eigenvector one; in the fit to the actual data, zone 3 is allowed to absorb all components. Also shown is the expected contribution of the cosmic X-ray background to the *Suzaku* PIN band (d) included in the model.

3 fully covering warm absorbers

1 ionized absorber fully covering the distant reflection component

( $N_H \sim 5 \times 10^{23} \text{ cm}^{-2}$ ,  $\log \xi \sim 2.0$ )

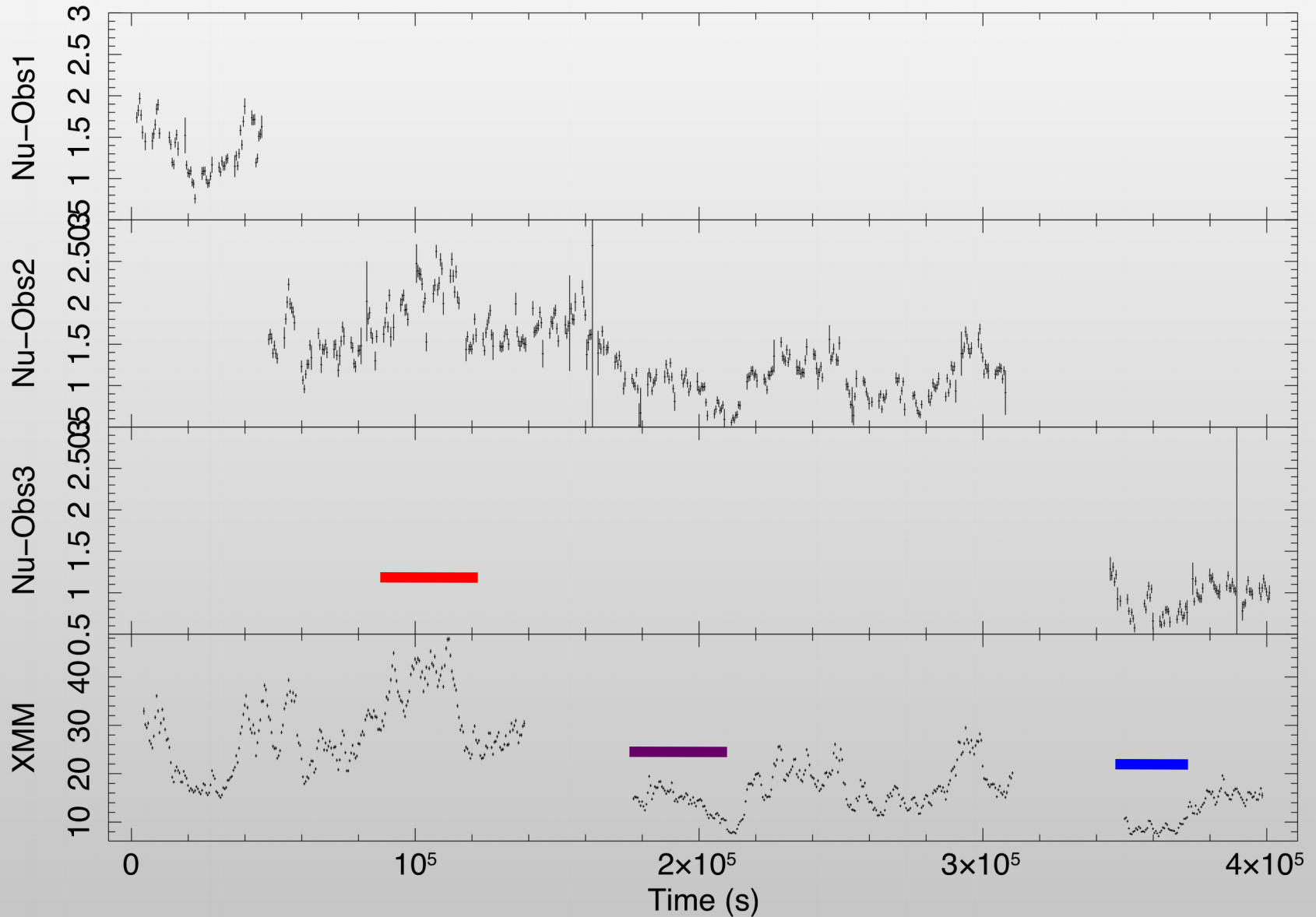
1 ionized absorber partial covering the X-ray source  
 ( $N_H \sim 4 \times 10^{22} \text{ cm}^{-2}$ ,  $\log \xi \sim 1.5$ )

- Brief introduction on MCG-6-30-15
- **The XMM-NuSTAR 2013 observational campaign**
- Testing the two different scenarios
  - Results
- Conclusions and future perspectives



# NuSTAR-XMM light curves

Bin time: 500.0 s

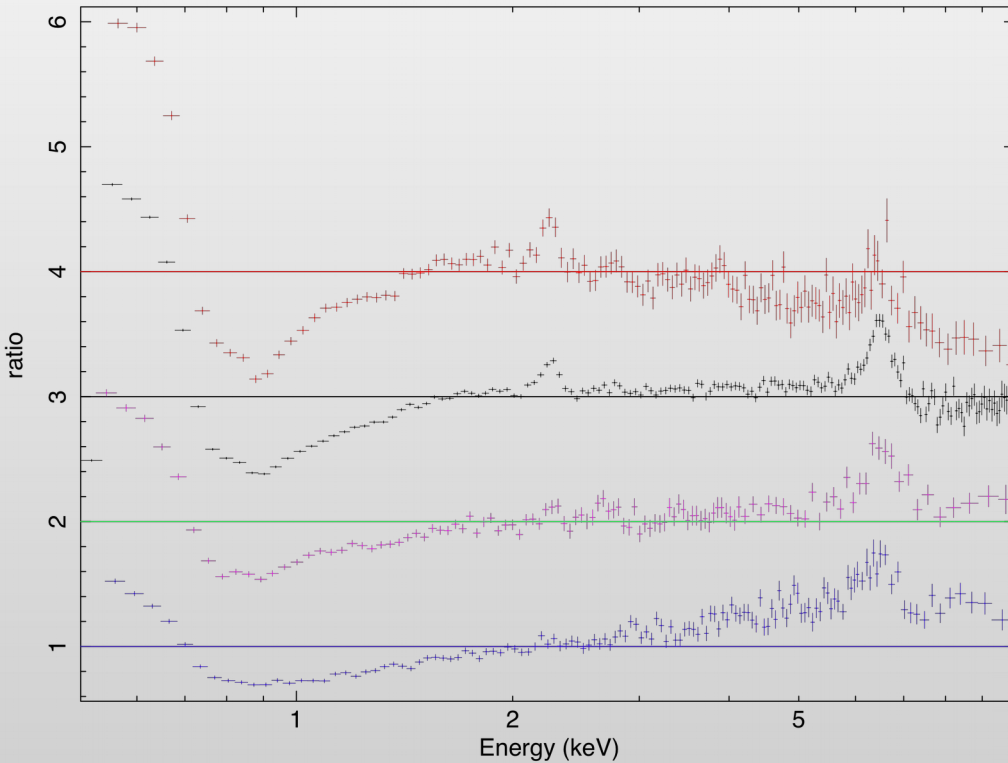


Start Time 16321 11:31:48:434 Stop Time 16326 2:21:48:434

# Spectral features

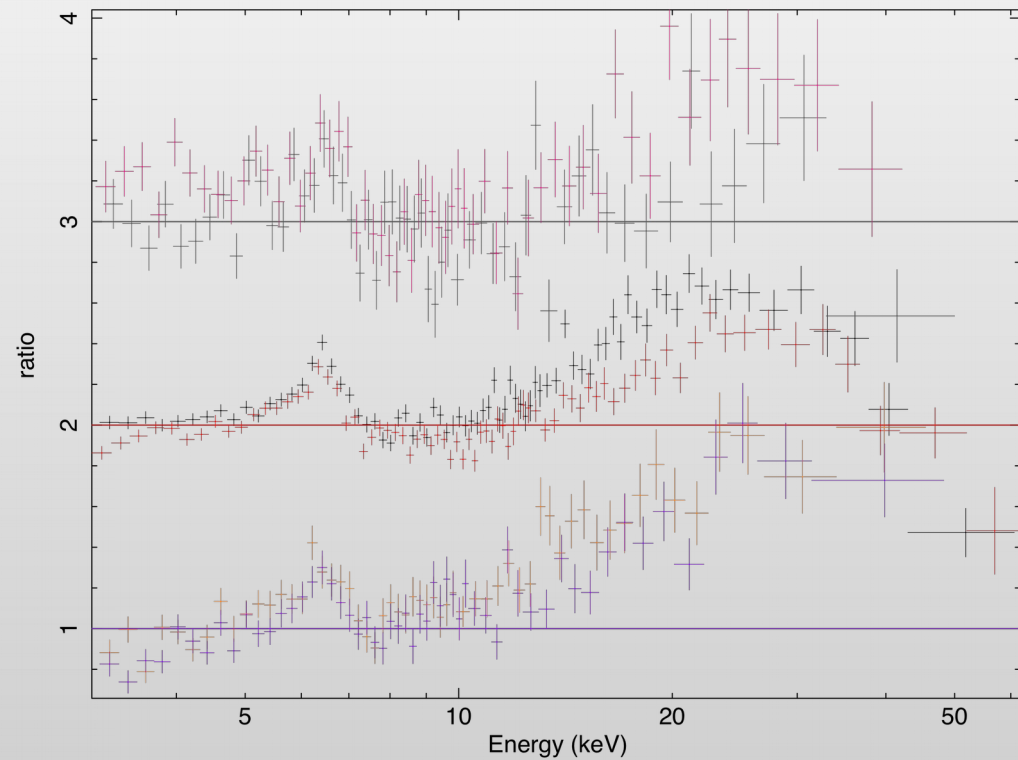
XMM-Newton EPIC-Pn

data/model



NuSTAR FpmA-FpmB

data/model



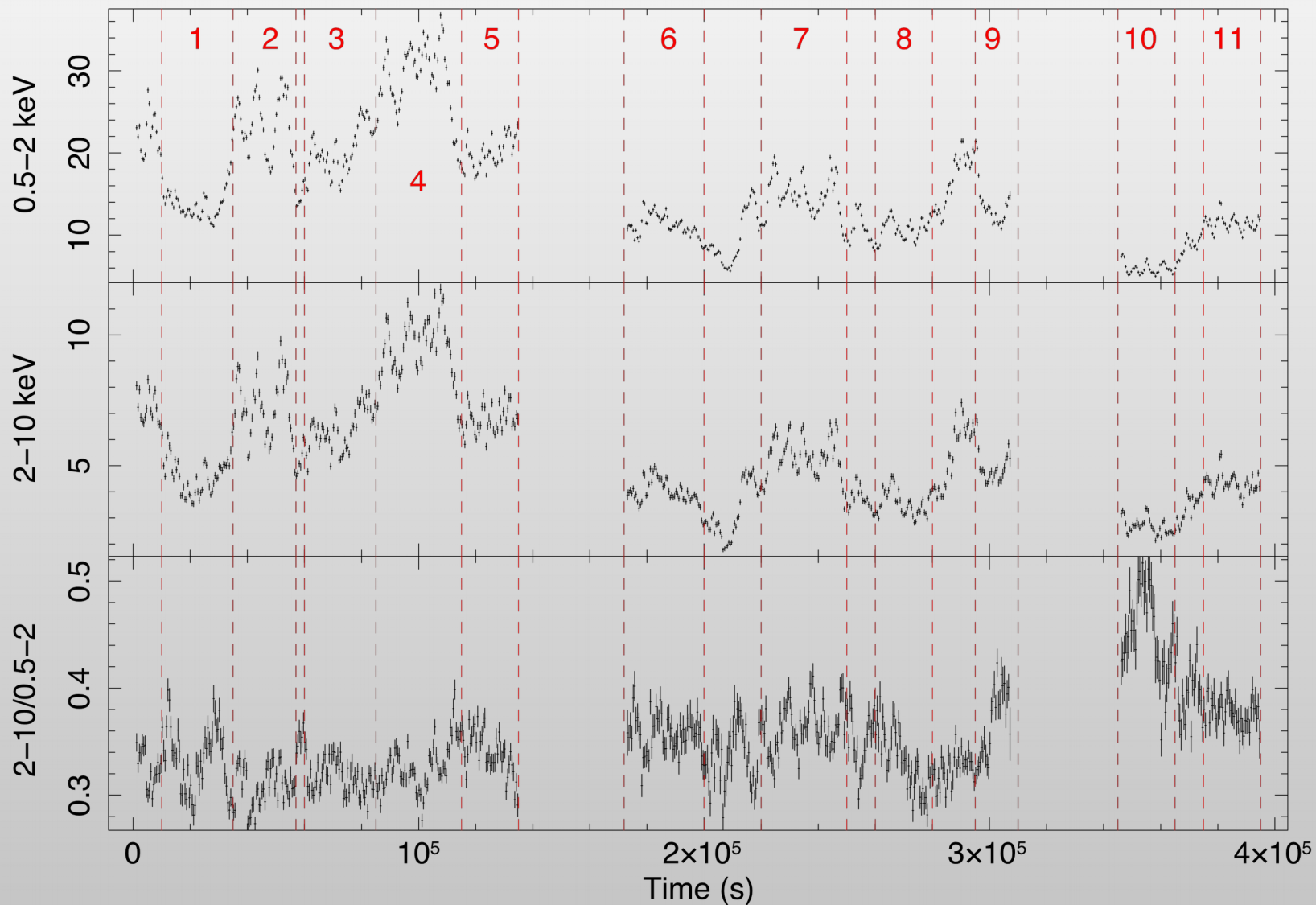
A broad Iron line, an intense soft excess and a strong Compton hump are present in the low flux spectrum (fit to a  $\Gamma=2$  power law).

- Brief introduction on MCG-6-30-15
- The XMM-NuSTAR 2013 observational campaign
- Testing the two different scenarios
  - Results
- Conclusions and future perspectives

# Fitting strategy

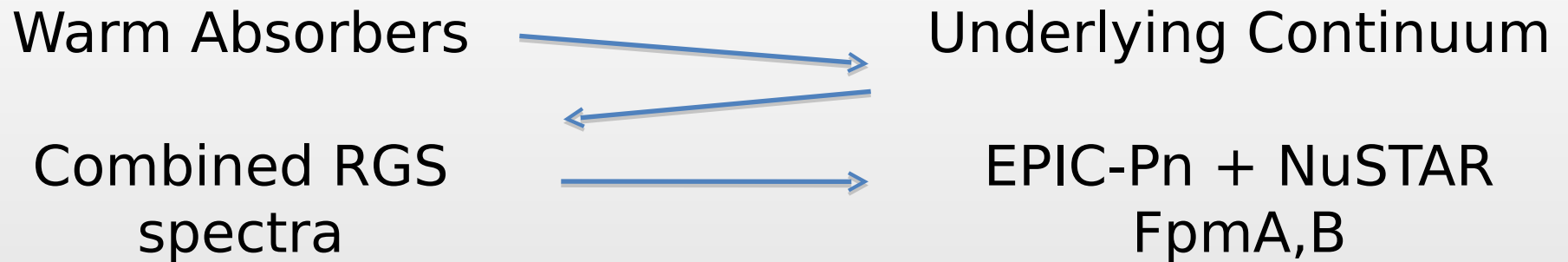
MCG-6-30-15: EPIC Pn light curves and time intervals

Bin time: 500.0 s



Start Time 16321 12:19:45:042 Stop Time 16326 1:38:05:042

# Fitting strategy



**REFLECTION**

**ABSORPTION**

$2 * XSTAR * DUST$

x

$(XILLVER + RELCONV * XILLVER + ZPOW)$

$2 * XSTAR * DUST$

x

$(XSTAR * XILLVER + XSTAR * ZPO + ZPO)$

XSTAR tables

XILLVER instead of REFLIONX:

<http://hea-www.cfa.harvard.edu/~javier/xillver/>

Iron UTA tables for dust

RELCONV for relativistic blurring:

[http://www.sternwarte.uni-](http://www.sternwarte.uni-erlangen.de/~dvoeuer/research/relconv/)

# Combined RGS1+2 analysis

$$N_{\text{H}1} = (4.6 \pm 0.8) \times 10^{20} \text{ cm}^{-2}$$

$$\log \xi_{\text{S}1} = 1.47 \pm 0.2$$

$$v \sim 2000 \text{ km s}^{-1}$$

$$N_{\text{H}2} = (1.3 \pm 0.2) \times 10^{20} \text{ cm}^{-2}$$

$$\log \xi_{\text{S}2} = 0.08 \pm 0.10$$

$$N_{\text{H}3} = (1.00 \pm 0.04) \times 10^{22} \text{ cm}^{-2}$$

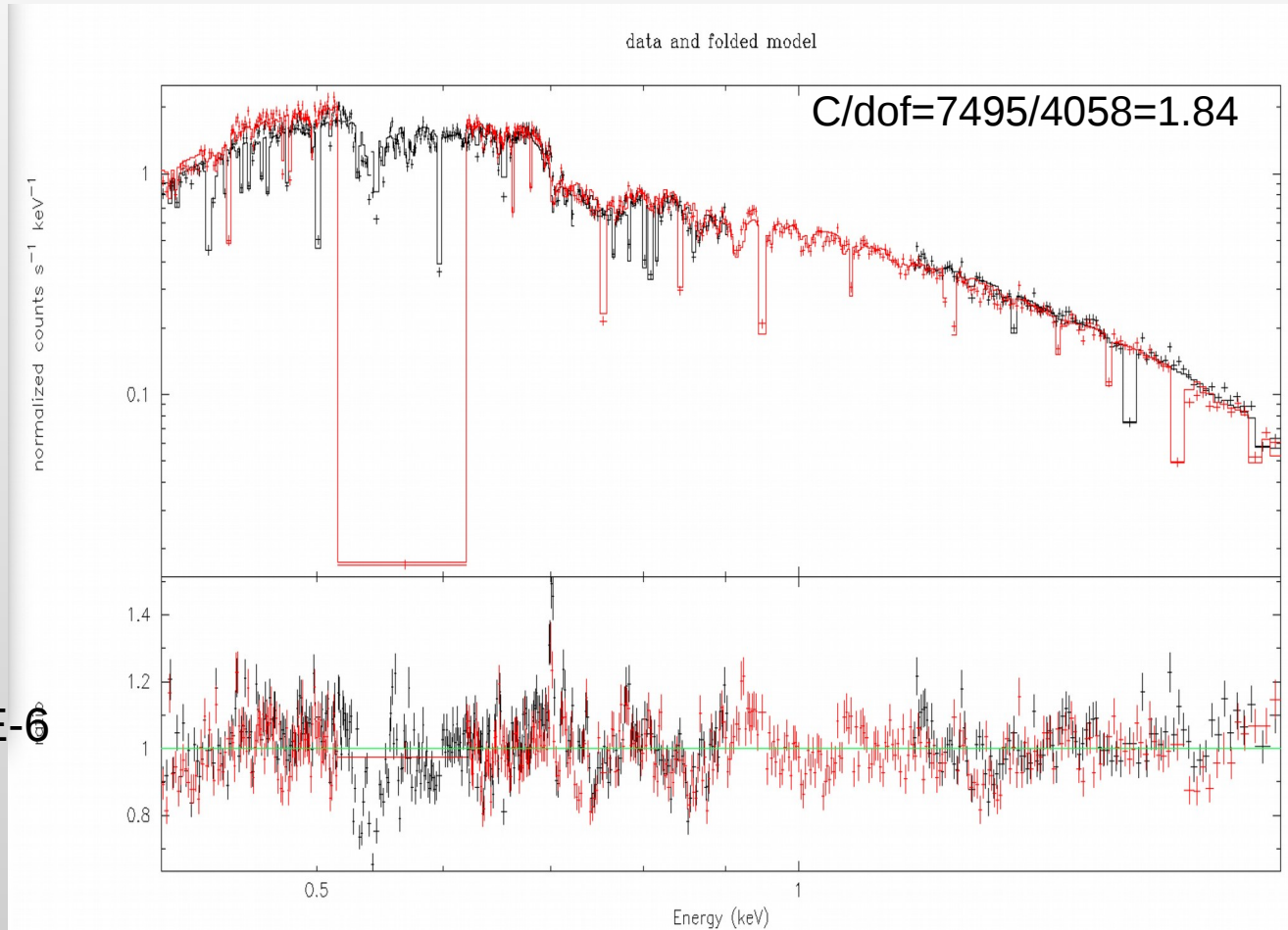
$$\log \xi_{\text{S}3} = 2.03 \pm 0.01$$

$$\log N_{\text{Fe}} = 17.32 \pm 0.02$$

$$\text{xillver Norm} = 9.3\text{E-}06 \pm 0.8\text{E-}6$$

$$\Gamma = 2.03 \pm 0.02$$

$$\text{norm} = 1.58\text{E-}02 \pm 0.02\text{E-}2$$



We then applied the combined best fit to the three separate RGS1+2 data sets

# Separate RGS1+2 analysis

## Orbit 1

$N_{H1}$  (5.6 +/- 1.7) x10<sup>20</sup> cm<sup>-2</sup>  
 $\log \xi_1$  1.82 +/- 0.05  
 $v \sim 2000$  km s<sup>-1</sup>  
 $N_{H2}$  (8.6 +/- 1.8) x10<sup>20</sup> cm<sup>-2</sup>  
 $\log \xi_2$  1.47 +/- 0.05  
 $N_{H3}$  (1.00 +/- 0.04) x10<sup>22</sup> cm<sup>-2</sup>  
 $\log \xi_3$  2.04 +/- 0.01  
 $\log N_{Fe}$  17.33 +/- 0.02

xillver norm 9.3E-06 +/- 0.8E-06  
 $\Gamma = 2.03^*$   
 norm 1.58E-02 +/- 0.02E-2

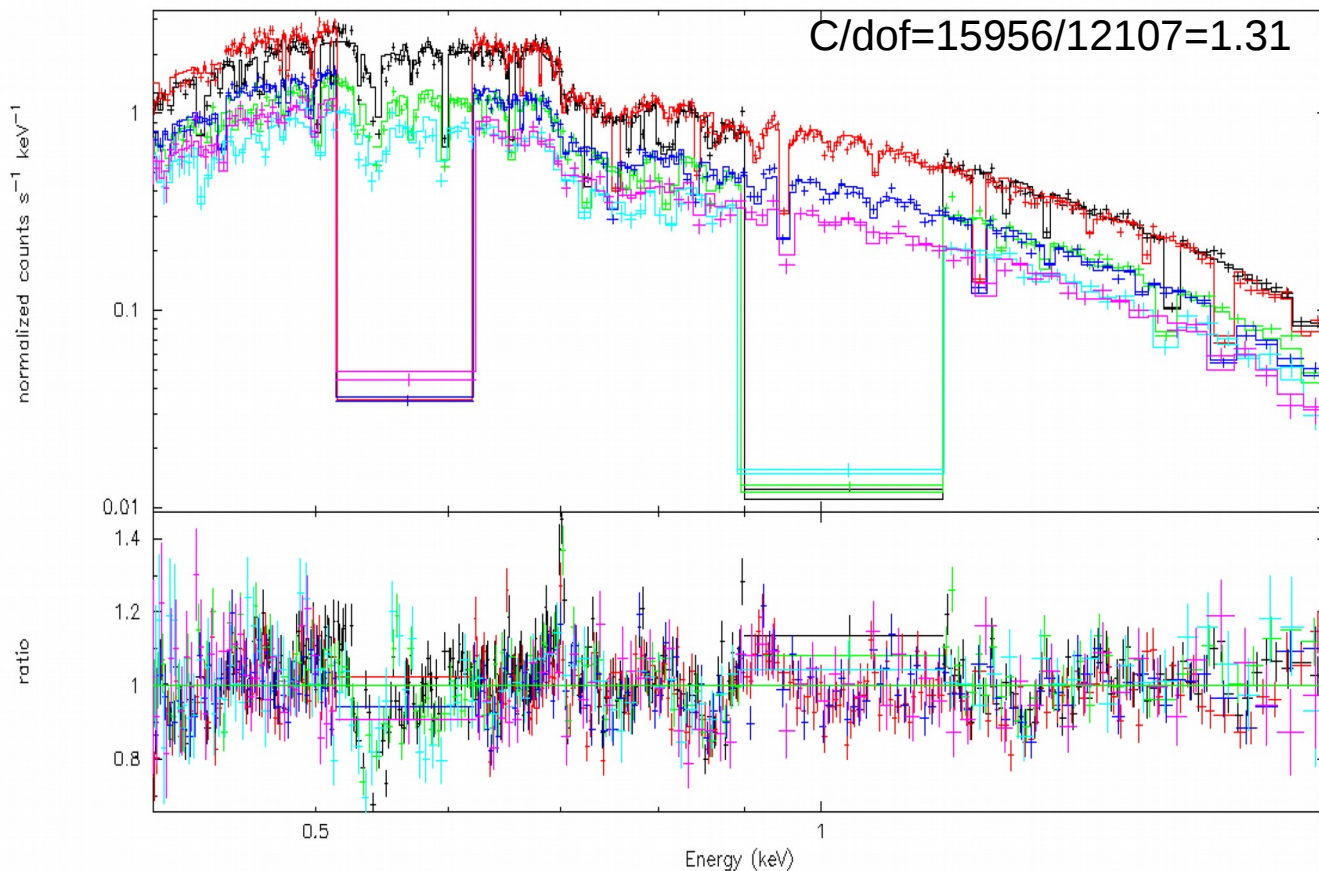
## Orbit 2

$N_{H1}$  (4.0 +/- 1.8) x10<sup>20</sup> cm<sup>-2</sup>  
 $\log \xi_1$  1.85 +/- 0.1  
 $v \sim 2000$  km s<sup>-1</sup>  
 $N_{H2}$  (2.9 +/- 0.5) x10<sup>20</sup> cm<sup>-2</sup>  
 $\log \xi_2$  1.34 +/- 0.13  
 $N_{H3}$  (1.00 +/- 0.09) x10<sup>22</sup> cm<sup>-2</sup>  
 $\log \xi_3$  2.02 +/- 0.02  
 $\log N_{Fe}$  17.27 +/- 0.04

$\Gamma = 2.03$   
 norm 1.22E-02 +/- 0.02E-02

No significant variation has been found in the warm absorbing structure

data and folded model



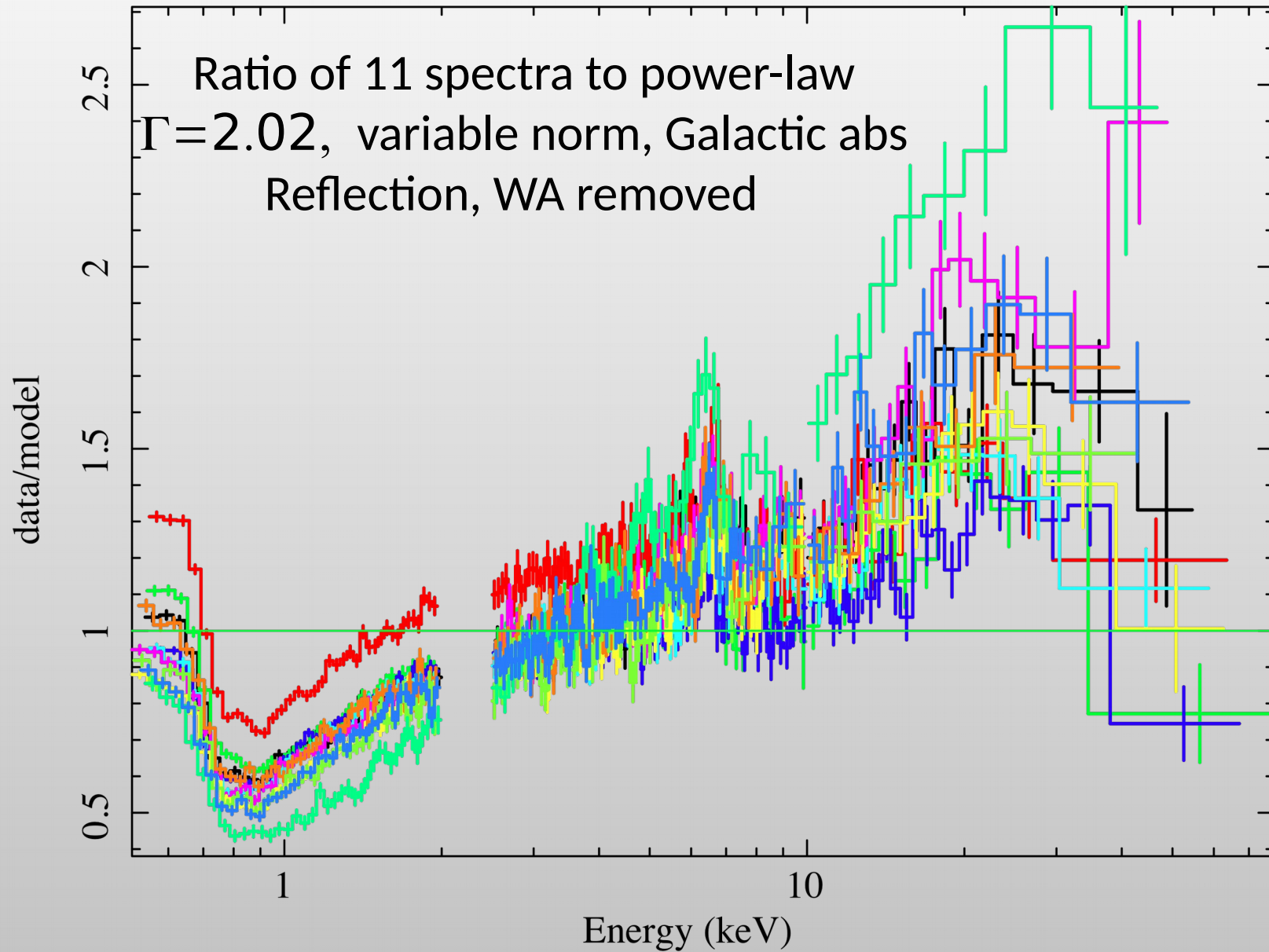
$N_{H1}$  (5.1 +/- 2.5) x10<sup>20</sup> cm<sup>-2</sup>  
 $\log \xi_1$  1.75 +/- 0.23  
 $v \sim 2000$  km s<sup>-1</sup>  
 $N_{H2}$  (5.0 +/- 1.0) x10<sup>20</sup> cm<sup>-2</sup>  
 $\log \xi_2$  1.3 +/- 0.3

$N_{H3}$  (0.88 +/- 0.02) x10<sup>22</sup> cm<sup>-2</sup>  
 $\log \xi_3$  2.00 +/- 0.03  
 $\log N_{Fe}$  17.08 +/- 0.12

$\Gamma = 2.03$   
 norm 0.8E-02 +/- 0.4E-03

## Orbit 3

# Time resolved simultaneous analysis





- Brief introduction on MCG-6-30-15
- The XMM-NuSTAR 2013 observational campaign
- Testing the two different scenarios
  - **Results**
- Conclusions and future perspectives

# Results: reflection

## Warm absorbers

$$N_{H1} = (0.6-2.5) \times 10^{22} \text{ cm}^{-2}$$

$$\log \xi_{S1} = 1.98 \pm 0.01$$

$$N_{H2} = (0.5-3.0) \times 10^{21} \text{ cm}^{-2}$$

$$\log \xi_{S2} = 1.27 \pm 0.02$$

$$\log N_{Fe} = 16.6 \pm 0.2$$

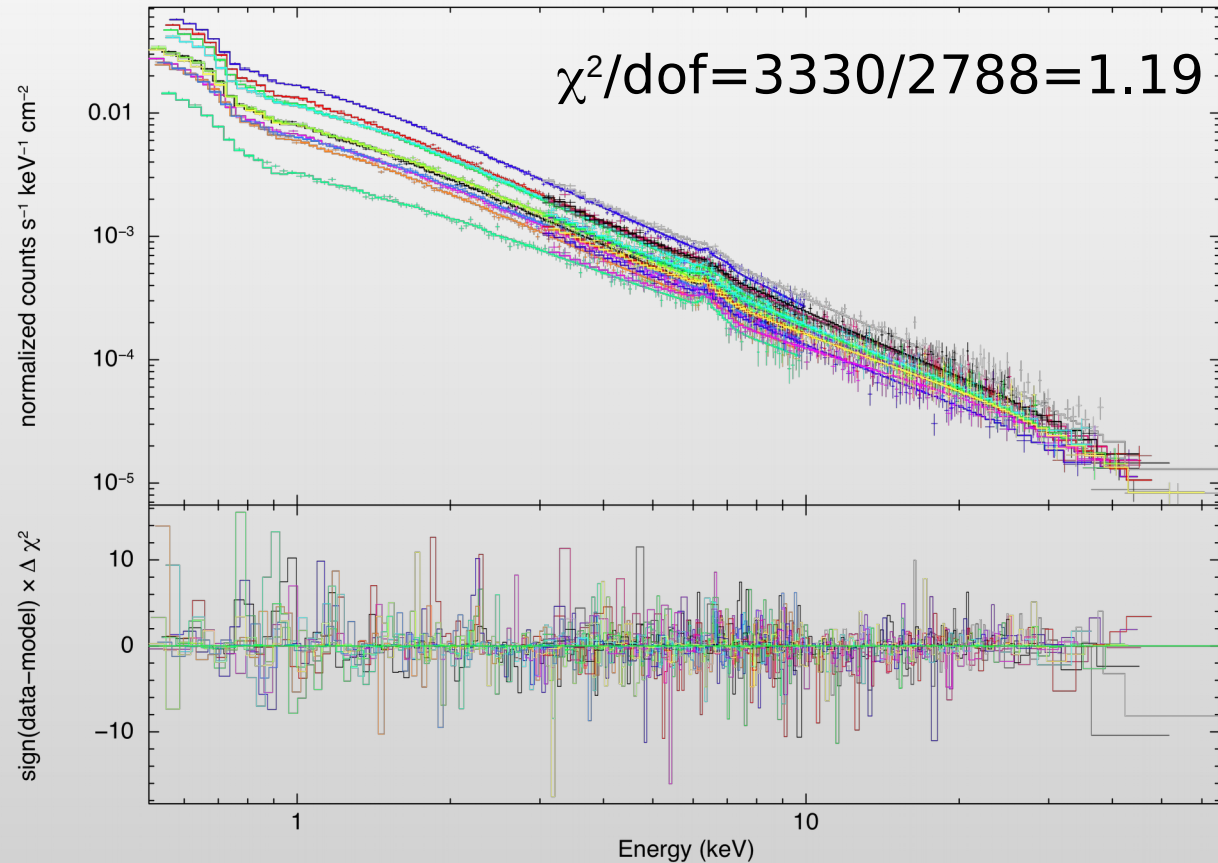
## Reflection parameters

$$(q=3.0 \text{ } a=0.998 \text{ } \text{incl}=37^\circ)$$

$$\log \xi = 0.2-3.0$$

$$A_{Fe} = 1.56 \pm 0.32$$

MCG-6-30-15: Broadband best fit

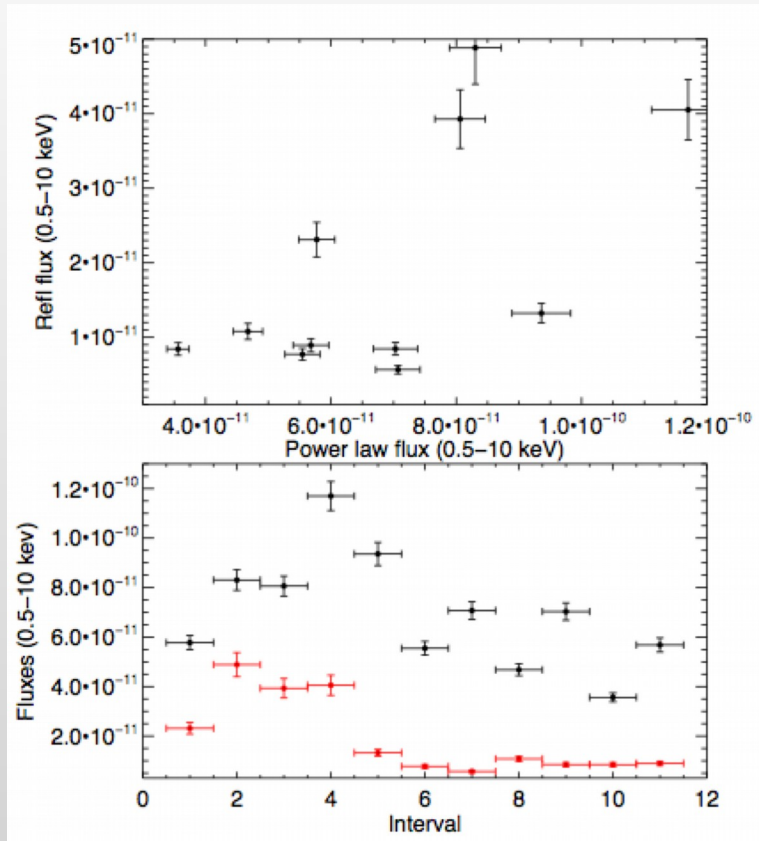


## Primary emission parameters

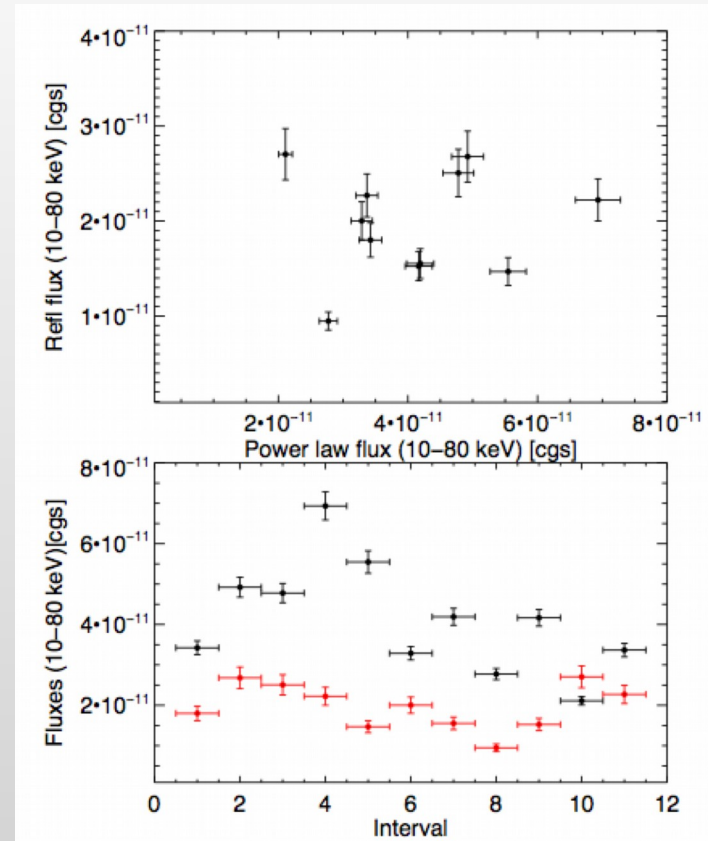
$$\Gamma = 2.050 \pm 0.005$$

$$E_c > 100 \text{ keV}$$

# RDC vs PLC fluxes



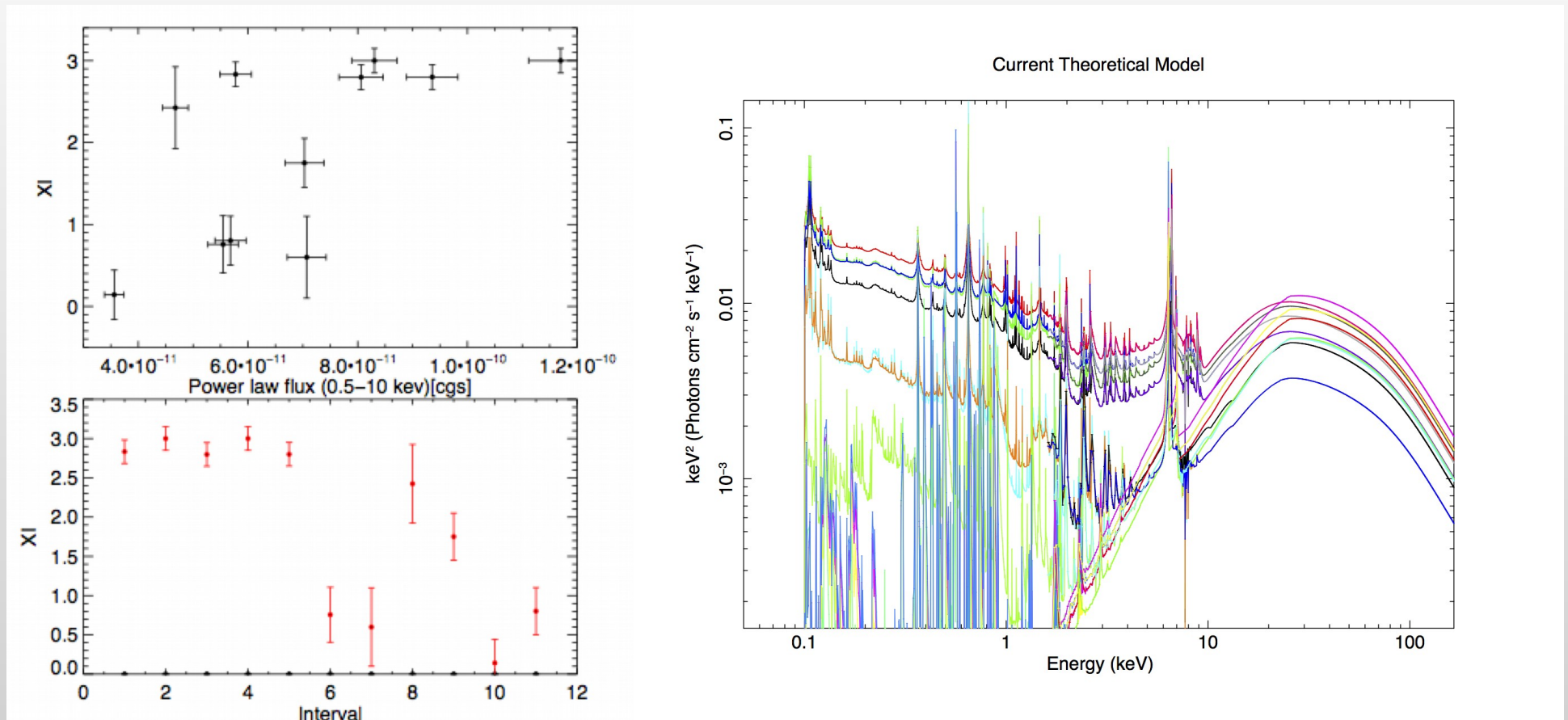
Variation of a factor  $\sim 2$  observed in the RDC between 0.5-10 keV, in agreement with the PCA (Parker et al., submitted)



Constancy of the RDC between 10-80 keV (thanks to NuSTAR)

Marginal response from the accretion disk to the nuclear emission?

# Accretion disk response



There is a response of the ionization state of the accretion disk to the variation of the PLC

# Results: absorption

## 2 warm absorbers

$$N_{H1} = (1.3 \pm 0.2) \times 10^{22} \text{ cm}^{-2}$$

$$\log \xi_{S1} = 1.95 \pm 0.02$$

$$N_{H2} = (4.2 \pm 1.5) \times 10^{21} \text{ cm}^{-2}$$

$$\log \xi_{S2} = 2.82 \pm 0.05$$

$$\log N_{Fe} = 16.9 \pm 0.1$$

## Further absorbers

$$(\text{Xillver: } \log \xi = 2.4 \pm 0.05; \quad \checkmark)$$

$$A_{Fe} = 0.5 \pm 0.1_p$$

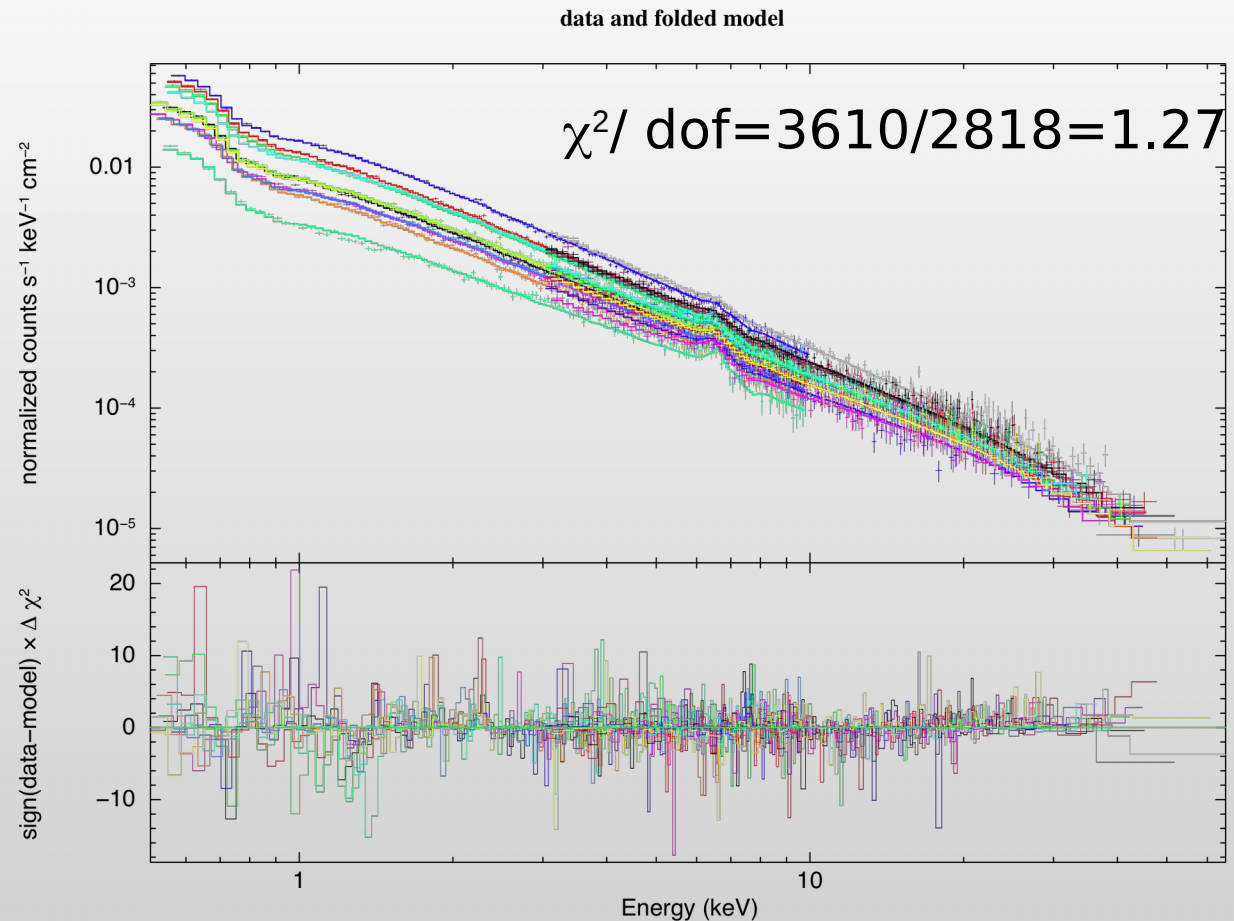
$$N_{H3} = (3.0 \pm 0.4) \times 10^{23} \text{ cm}^{-2} \quad \checkmark$$

$$\log \xi_{S3} = 2.11 \pm 0.01$$

$$N_{H4} = (0.3-27) \times 10^{21} \text{ cm}^{-2}$$

$$\log \xi_{S4} = (0.0015 \pm 0.0005) \quad \times$$

[almost neutral]



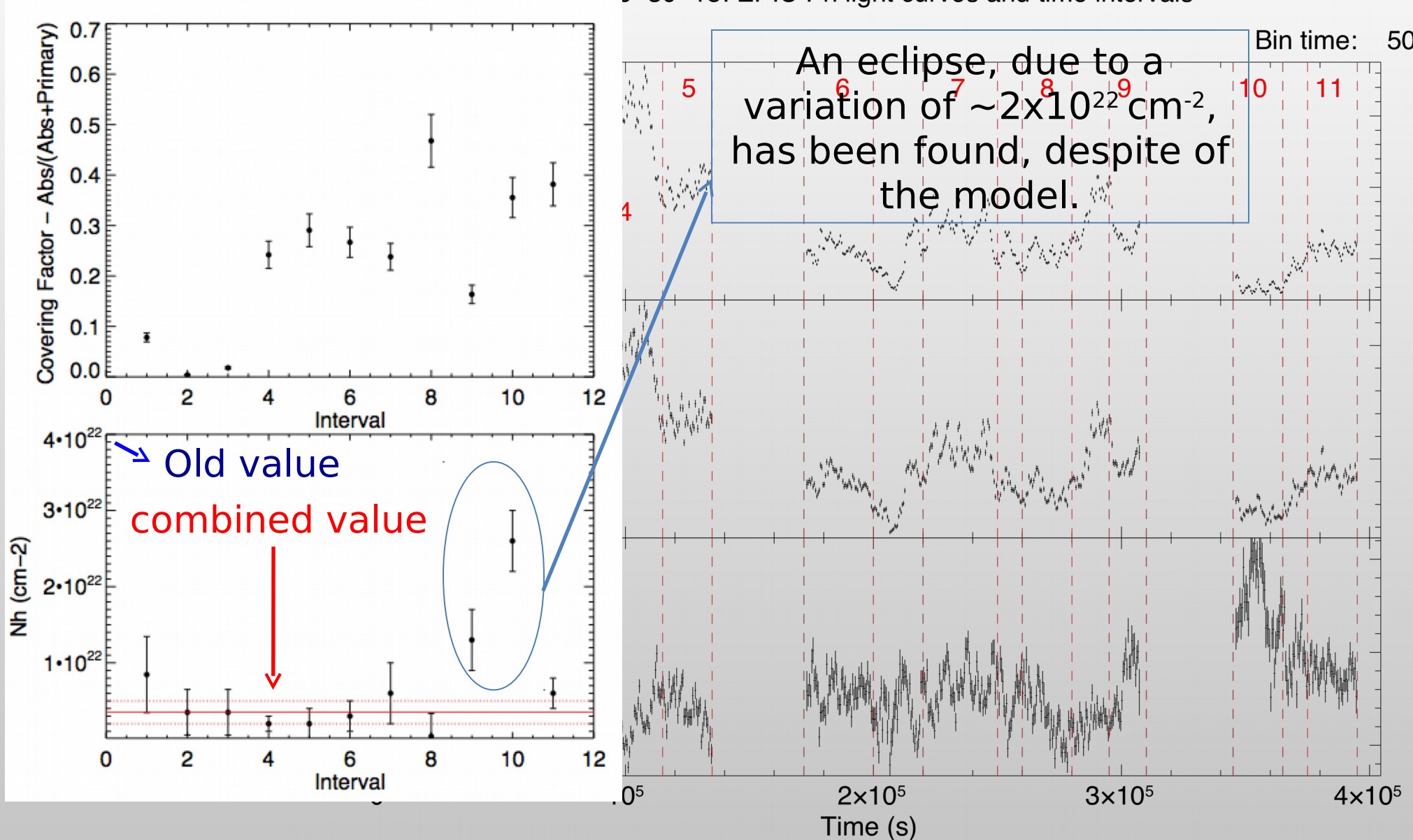
## Primary emission parameters

$$\Gamma = 2.16 \pm 0.01$$

$$E_c > 100 \text{ keV}$$

# Covering factor time evolution

MCG-6-30-15: EPIC Pn light curves and time intervals



Start Time 16321 12:19:45:042 Stop Time 16326 1:38:05:042

- Brief introduction on MCG-6-30-15
- The XMM-NuSTAR 2013 observational campaign
  - Testing the two different scenarios
    - Results
- **Conclusions and future perspectives**

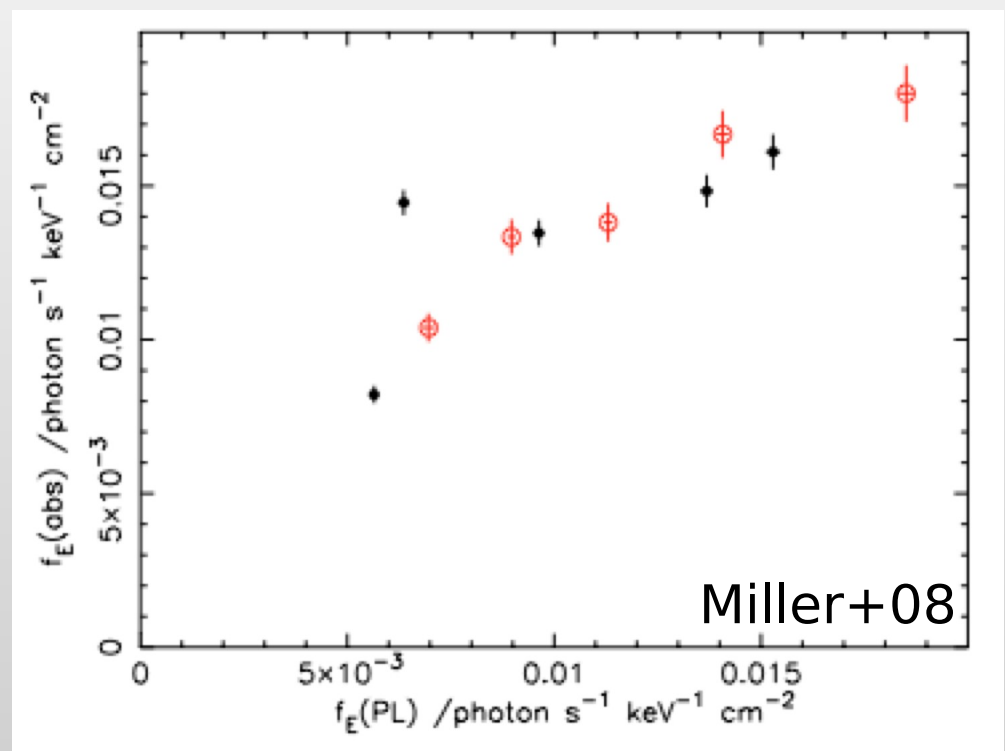
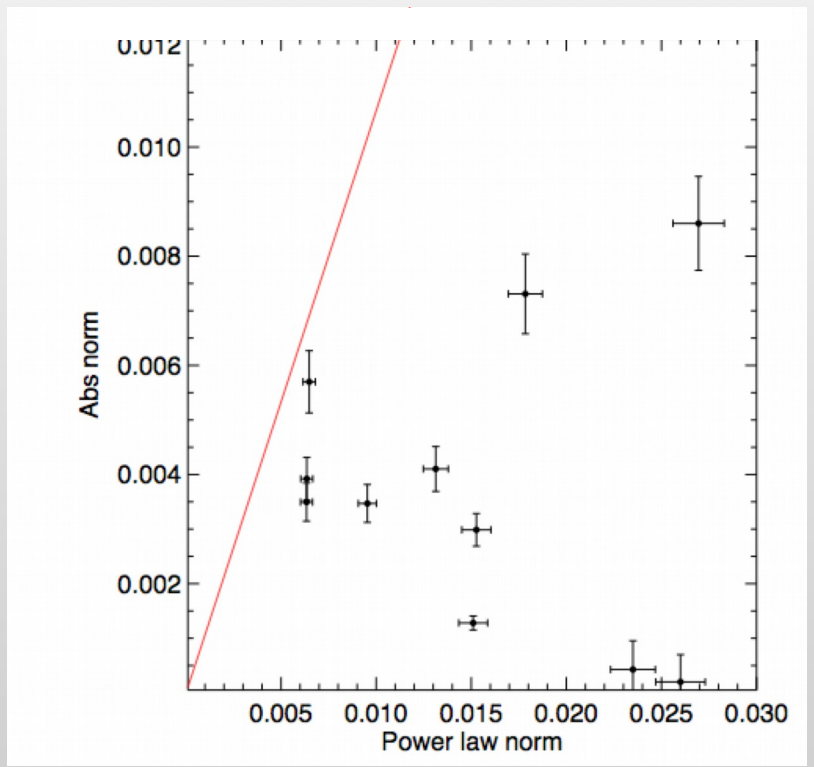
# Conclusions

- The warm absorbing structure is consistent with literature, except for the lack of highly ionized absorption lines;
- The reflection scenario well explains the behavior of the source, from **0.4 keV** up to **80 keV**
- Spectral variability can be explained in terms of strong variations of the PLC and to marginal variations in the RDC
- An alternative is that the spectral variability can be attributed to a change in covering fraction of the X-ray source AND to a change of  $N_{\text{H}}$ .
- Clear evidence of BLR eclipses have been found



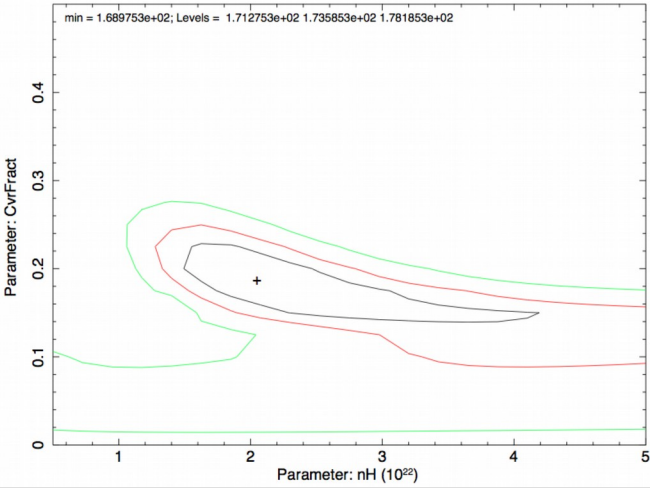


# Backup

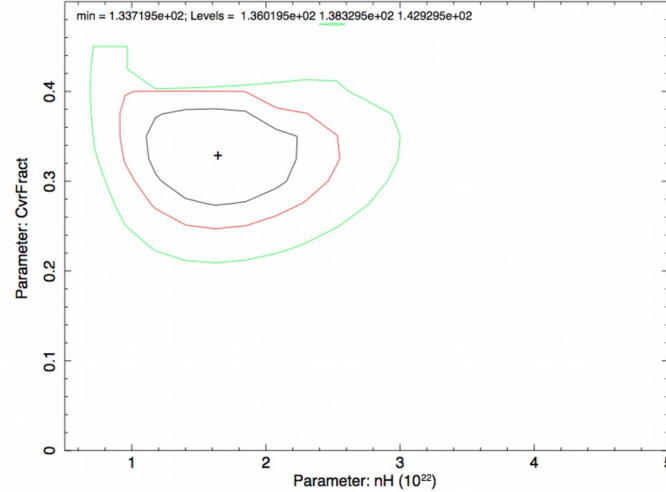


# Backup

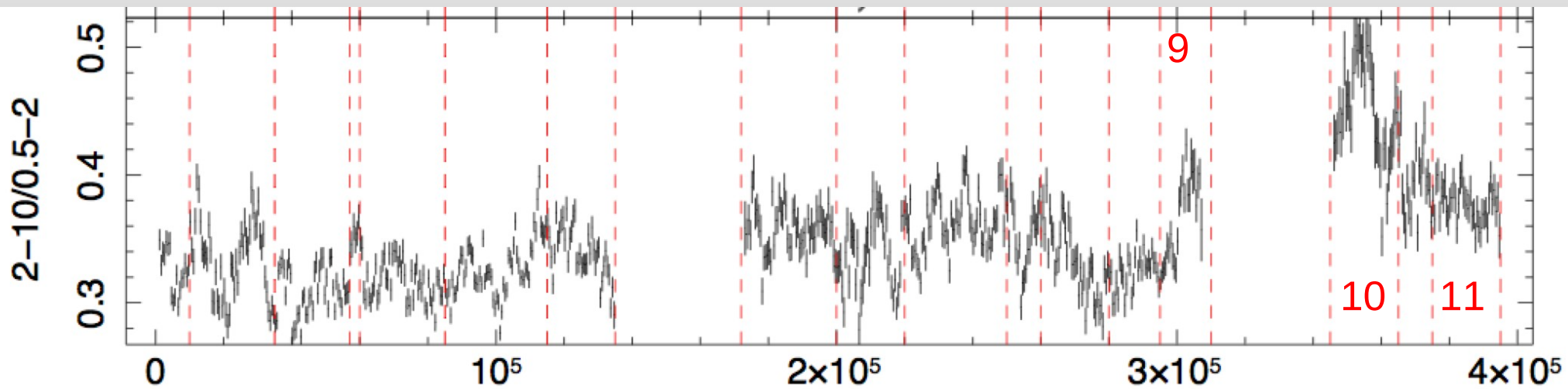
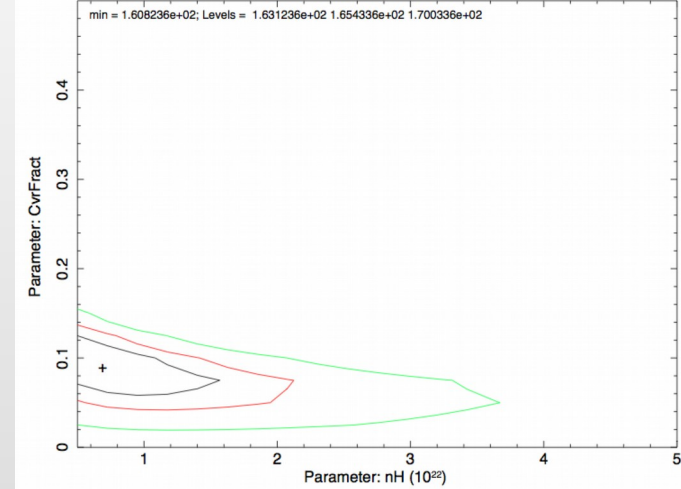
Confidence contours: INTERVAL 9



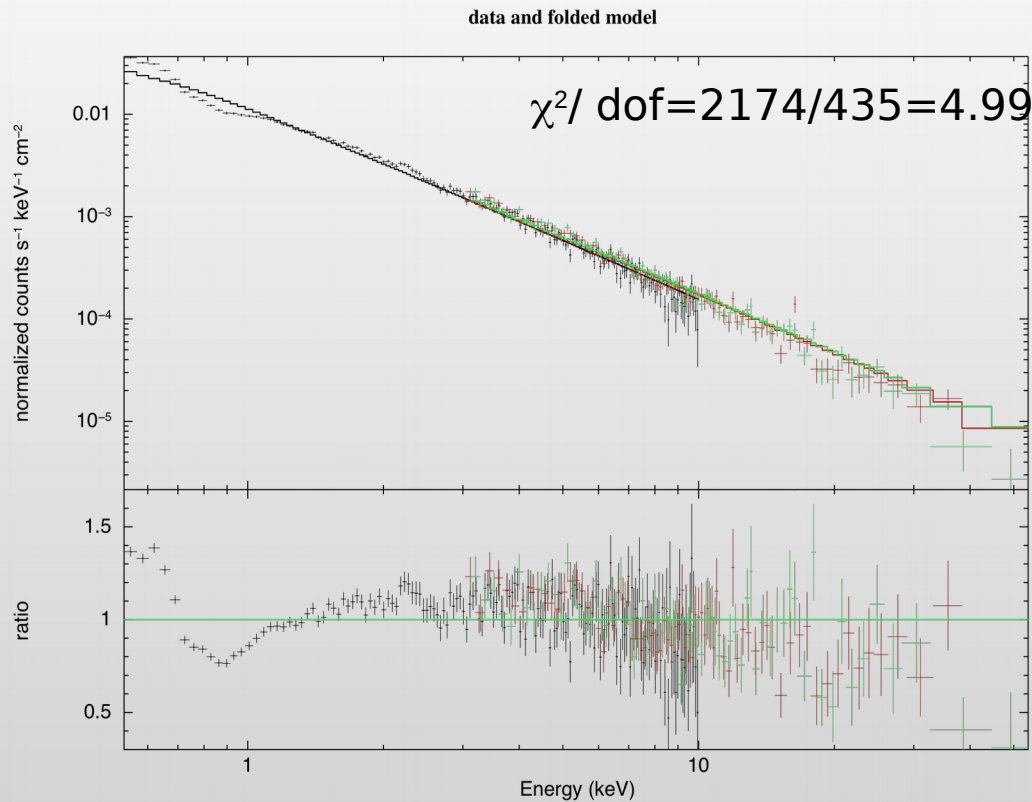
Confidence contours: INTERVAL 10



Confidence contours: INTERVAL 11

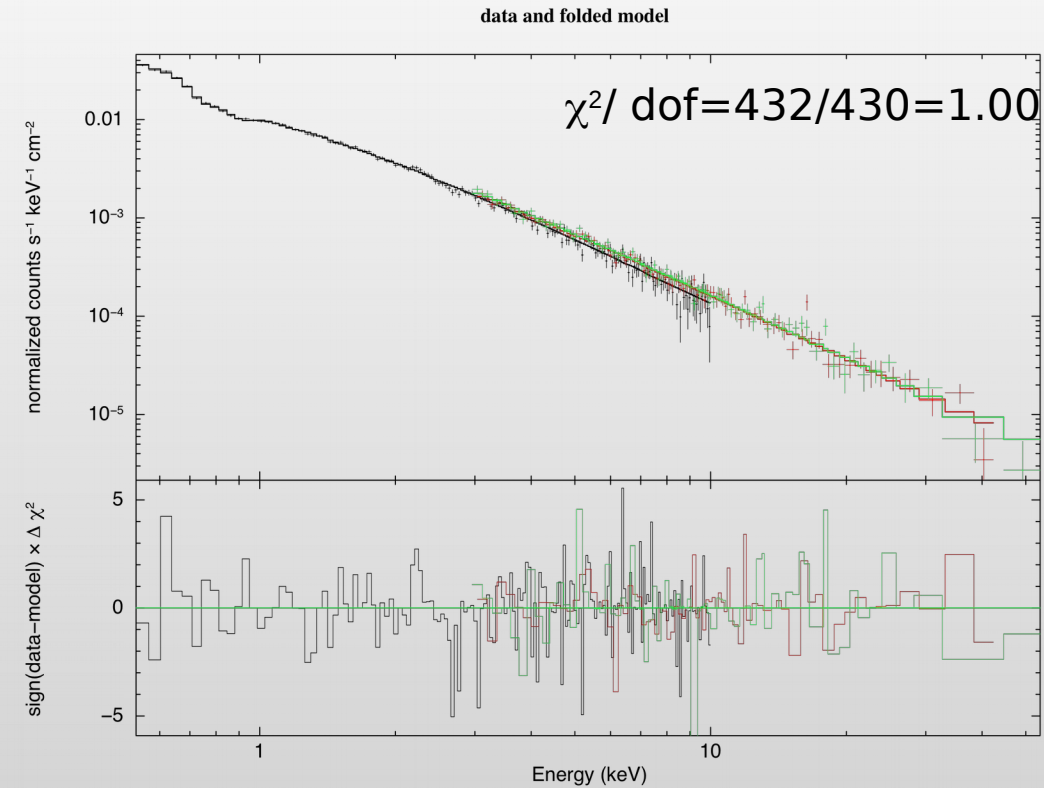


# Backup



Difference between the highest flux spectrum ( $42.19 \pm 0.07$  cts/s) and a low flux one with constant HR ( $17.79 \pm 0.04$  cts/s)

A first fit with an absorbed power law leads to strong residuals, mainly due to the warm absorbing structure



$$N_{\text{H}1} = (9.8 \pm 2.5) \times 10^{21} \text{ cm}^{-2}$$
$$\log \xi_1 = 2.0 \pm 0.1 \quad \Gamma = 2.16 \pm 0.03$$

$$N_{\text{H}2} = (2.1 \pm 1.9) \times 10^{21} \text{ cm}^{-2}$$
$$\log \xi_2 = 1.4 \pm 0.2$$

$$\log N_{\text{Fe}} = 17.2 \pm 0.3$$